Enhancing Efficiency in Hybrid Solar–Wind–Battery Systems Using an Adaptive MPPT Controller Based on Shadow Motion Prediction

Abdorreza Alavi Gharahbagh [1], **Vahid Hajihashemi** [1], **Nasrin Salehi** [2], **Mahyar Moradi** [3], **José J. M. Machado** [4] **and João Manuel R. S. Tavares** [4,*]

1. Faculdade de Engenharia, Universidade do Porto, Rua Dr. Roberto Frias, s/n, 4200-465 Porto, Portugal; abalavi.gh@gmail.com (A.A.G.); hajihashemi.vahid@ieee.org (V.H.)
2. Department of Basic Sciences, Shahrood Branch, Islamic Azad University, Shahrood 36199-43189, Iran; salehi9002@gmail.com
3. Department of Electrical and Computer Engineering, Shahrood Branch, Islamic Azad University, Shahrood 36199-43189, Iran; mahyar.moradi630@yahoo.com
4. Instituto de Ciência e Inovaç ao em Engenharia Mecânica e Engenharia Industrial, Departamento de Engenharia Mecânica, Faculdade de Engenharia, Universidade do Porto, Rua Dr. Roberto Frias, s/n, 4200-465 Porto, Portugal; jjmm@fe.up.pt
*   Correspondence: tavares@fe.up.pt; Tel.: +351-22-041-3472

Abstract: Renewable energy sources are particularly significant in global energy production, with wind and solar being the most prevalent sources. Managing the simultaneous connection of wind and solar energy generators to the smart grid as distributed generators involves complex control and stabilization due to their inherent uncertainties, making their management more intricate than traditional power plants. This study focuses on enhancing the speed and efficiency of the maximum power point tracking (MPPT) system in a solar power plant. A hybrid network is modeled, comprising a wind turbine with a doubly-fed induction generator (DFIG), a solar power plant with photovoltaic (PV) cells, an MPPT system, a Z-source converter, and a storage system. The proposed approach employs a motion detection-based method, utilizing image-processing techniques to optimize the MPPT of PV cells based on shadow movement patterns within the solar power plant area. This method significantly reduces the time required to reach the maximum power point (MPP), lowers the computational load of the control system by predicting shadow movements, and enhances the MPPT speed while maintaining system stability. The approach, which is suitable for relatively large solar farms, is implemented without the need for any additional sensors and relies on the system's history. The simulation results show that the proposed approach improves the MPPT system's efficiency and reduces the pressure on the control circuits by more than 70% in a 150,000 m^2 solar farm under shaded conditions.

Keywords: DFIG; wind turbine; Z-source converter; solar farm; motion prediction; MPPT

1. Introduction

In recent decades, the increasing generation of electricity from distributed sources has reduced fossil fuel consumption. Wind turbines and photovoltaic (PV) systems are two of the most prominent forms of distributed generation. One of the limitations of these systems involves the uncertainties caused by natural wind and sun variations. These uncertainties highlight the need for properly and optimally designed wind and solar energy production units to handle various situations [1]. Wind turbines come in two varieties: fixed speed or variable speed. With the fixed speed type, changing the rotor speed by 1% and connecting it directly to the network is possible. The rate is often stabilized in proportion to the network frequency in the fixed speed type, and the wind speed affects the voltage. Wind fluctuations impact the performance and output voltage of this type

of turbine. Controlling the rotor speed is possible in variable-speed turbines where the generator is controlled by electronic power equipment. By changing the rotor speed, the effect of wind fluctuations is dissipated. Variable speed generators allow changing the rotational velocity over a wide range. These generators can be classified into two types based on their connection to the network—either direct or indirect—their overall power level, or the conversion deficit used for the generator [2]. However, connecting indirectly to the network typically involves using a full-power converter, whereas a direct connection generally employs a low-power converter. Electrical system options for variable-speed or fixed-speed wind turbine generator operations are usually categorized based on the layout of the converters and the machine's inherent characteristics. Wind system generators are commonly classified as direct current (DC) generators [3], induction generators [4], doubly-fed induction generators (DFIGs) [5], synchronous generators [6], and switched reluctance generators [7].

Solar energy is considered an alternative to wind energy for reducing the use of fossil and nuclear fuels and promoting a cleaner environment. Solar energy possesses naturally stored potential energy that can be harnessed to generate various forms of energy, such as electrical, thermal, and chemical [8]. Solar energy is expandable and typically self-sufficient. Recently, hybrid systems, such as PV and wind turbines, have received much attention. However, the output fluctuation of these hybrid systems remains a challenge [9,10]. For the first time in the European Union (EU), the growth of electricity generation from new energy sources surpassed the development of fossil fuels in 2006. Wind power generation capacity increased from 18,000 to 92,000 MW between 2000 and 2007. Despite global economic growth of only 1–2% per year since 2000, the industry has grown by 25%, doubling every three years.

Wind power plants have been extensively researched across various fields [11]. One of these areas involves the control of wind turbines. When data from 2009 to 2013 are compared, there is a 54% increase in the volume of energy received in megawatts from wind turbines, with industrialized countries currently leading the way [12]. However, the structure and performance of wind turbine systems depend highly on their mechanical properties, such as the axis of the rotation gearbox and the control system [13–15].

On the other hand, EU solar generation capacity has continued to increase, reaching an estimated 259.99 GW in 2023, according to SolarPower Europe (Brussels, Belgium). However, due to the variable nature of solar radiation, which can be affected by clouds and shadows, PV systems require a controller to operate at maximum power point (MPP). Therefore, numerous studies have been conducted on maximum power point tracking (MPPT) algorithms.

2. Literature Review

2.1. Wind Turbine Generators

Like all electric generators, a wind turbine generator converts energy, known as wind mechanical energy, into electrical energy. Wind turbine generators are different from other grid-connected generators. The main difference is that a wind turbine generator has to work with wind energy that supplies fluctuating torque and mechanical power. There are different types of wind turbine generators, as follows:

- Synchronous generator with field winding—a synchronous generator typically consists of a three-phase winding stator that feeds the external load and a rotor that generates a magnetic field. The rotor may be magnetically permanent or have an area winding system [16].
- Permanent magnetic synchronous generator—with this type of generator, the incremental converter controls the electromagnetic torque. The converter regulates the direct current (DC) connection voltage and controls the input power factor on the power supply side. One of its drawbacks involves using a diode rectifier, which increases the current and distortion range [17].

- DFIG wired rotor generator—a DFIG controller can be a good solution for variable speed systems with a 30% synchronous speed change range. Furthermore, the power of the electronic power converter in these systems constitutes 20–30% of the total power of the generator, which contributes to lower losses compared to other types that operate at full power. Converter prices and costs are also reduced. The term "doubly-fed" refers to the stator supplying power to the power grid and the load, while the power converter generates the rotor voltage [18]. These systems have wide but limited operating speed ranges. The converter compensates for the difference in electrical and mechanical frequencies by injecting the variable frequency current into the rotor [19]. The power converters and controllers regulate the generator's behavior during both regular operation and faults. The advantages of a DFIG controller include the following: (a) the ability to control the reactive power, (b) the ability to independently control active and reactive capabilities, (c) the ability to be magnetized by the rotor, and (d) reactive power generation capability.
- DFIG all-control winding rotor generator—the controller used in these generators offers greater controllability flexibility than a traditional DFIG controller. These wind power systems are designed for wind farms located at sea and connected to neighboring land via sea cables. Other methods of integrating an induction generator into a grid include cycloconverters [20] and matrix converters [21]. The disadvantages of these systems include a low line power factor, high harmonic deviations in line and machine flow for cycloconverters, and the removal of DC capacitors in matrix converters. This type of converter is complex, and its technology needs to be more mature.
- Cage rotor induction generator—the stator windings in these generators are linked to the network via an electronic power converter. The stator converter control system regulates the electromagnetic torque and supplies the machine with reactive power [22]. The network side converter regulates the DC connection voltage and controls the active and reactive power transfer from the system to the network.
- A dual-stator winding induction generator [23]—the two stator windings are electrically isolated in these machines.
- Two-speed cage rotor induction generator—this type of generator increases the turbine's efficiency at low wind speeds, which is unsuitable for large wind farms because it cannot power the network [24].
- A DFIG field-oriented controller—this was used in Ref. [25] due to its ability to manage and optimize wind turbine speed and torque control. This controller divides the stator current into segments to produce the torque and flux.
- A DFIG vector control (VC) for grid and rotor side converters—this approach was suggested in [26], exploiting fuzzy controls such as Mamdani, Sugeno, and ANFIS.

2.2. Solar Cells

Palanivel et al. [27] used an ANFIS controller and a super lift boost converter for MPPT in a PV system. Hepzibah and Remkumar [28] used an ANFIS-PI controller for MPPT. In this study, the power generated by the PV cell was used to run a water pump and was not connected to the grid. Anbarasu et al. [29] used an ANFIS-based fractional order proportional–integral–derivative method to control a PV cell, which was connected to the grid through a DC-DC converter. Mahdi et al. [30] used perturb-and-observe (P&O), fuzzy logic, and ANFIS methods for MPPT in a PV cell with a boost DC-DC converter. The output of the system was connected to the grid. Hamouda et al. [31] used an ANFIS controller to control a PV cell and MPPT, where the particle swarm optimization (PSO) algorithm was used to design an ANFIS. The studied system included a brushless DC motor-based wire feeder unit. Farah et al. [32] compared a fuzzy logic-based and an ANFIS approaches for MPPT and evaluated their stability and speed in reaching the MPP. The study showed that using an ANFIS with reduced rules can improve system efficiency.

Javed et al. [33] compared the performance of ANFIS-based MPPT methods with non-fuzzy methods, demonstrating the capabilities of ANFIS-based approaches. Moyo

et al. [34] proposed an ANFIS-based method for MPPT in a PV system. The method uses a DC-DC boost converter. The dynamic response of PV systems to grid fluctuations was compared to conventional PV systems, demonstrating its effectiveness. Ibrahim et al. [35] used an ANFIS and DC-DC boost converter combination to control a PV cell and battery system. The solution takes into account the effects of grid disturbances and the control system's ability to mitigate them. Additionally, MPPT was integrated into the control system. Pareek and Kaur [36] proposed an ANFIS-PID-Based MPPT controller system in a setup comprising a PV cell to charge an electric vehicle. Pachaivannan et al. [37] used an ANFIS-assisted crowded plant height optimization for controlling a PV system under partial shading conditions. The control system employs a DC-DC boost converter. Bendary et al. [38] used two ANFIS controllers for fault detection and isolation and output control in a PV system. In a review article, Guerra et al. [39] examined various ANFIS methods employed to control PV systems. Among the discussed aspects were the types of converters used in controlling PV systems and the control objectives from the grid perspective. Ahmed et al. [40] enhanced the performance of an MPPT system in a setup comprising a PV cell and a battery by combining an ANFIS and a hybrid crow-pattern search algorithm. The authors studied the environmental effects on the PV cell's output and their impact on the controller.

Revathy et al. [41] used an ANFIS for MPPT. Additionally, the study included a DC-DC converter to connect the system to a DC grid. The capability of this solution under various weather and partial shading conditions was discussed. Subramaniam et al. [42] proposed a multi-input–output ANFIS-controlled solar-fuel-cell-based switched capacitor Z-source converter system for charging an electric vehicle. The system included a combination of a PV cell and a fuel cell to charge the vehicle's battery. Rahman et al. [43] built an organic solar supercapacitor structure for charging an electric vehicle. The control system was based on an ANFIS, and the employed converter was a pulse width modulation (PWM) DC-DC converter. Alaas et al. [44] studied the MPPT in a solar cell and battery system based on the sparrow search algorithm and an ANFIS. The suggested control system considers variations in solar irradiation, ambient temperature, and weather conditions. Sultana and Jebaseelan [45] proposed an ANFIS controller for transient and voltage stability enhancement of an inverter in a PV system. This controller simultaneously performs MPPT. A combination of a quasi-Z-source converter, DC link capacitor, three-phase voltage source inverter, MPPT controller, and a brushless DC drive was used in [46] to enhance the performance of a Solar PV Driven System.

Some studies have focused on maximizing power quality in systems with renewable energy sources. For example, Tehrani et al. [47] used a genetic algorithm to minimize harmonics in a microgrid with renewable energy sources and maximize power quality. In another study, Belgacem et al. [48] proposed a method for maximizing the efficiency of renewable energy sources through energy management from the consumer side. Since the goal was to maximize the output of renewable sources and minimize fluctuations during changes in renewable source inputs, energy management algorithms with demand-side management approaches were not considered.

Based on the review conducted, it is evident that the PV systems proposed thus far have either focused solely on MPPT for individual PV cells or have not considered solar farms. A comprehensive analysis of various conditions under different scenarios has not been performed for systems involving many PV cells across a wide area. Therefore, the present study aims to enhance existing solar farm-wind turbine-battery systems by considering predictable factors. The main contributions of this study are as follows:

- We improve existing solar farm systems by considering the shadow conditions and MPPT;
- We use motion detection to predict the shadow pattern in a solar farm;
- We propose an effective hybrid system, including PV and wind sources, using a combination of well-known DFIG, ANFIS, and Z-source converter components.

3. Theoretical Framework

3.1. Wind Turbines and DFIG Systems

DFIGs have received much attention in recent years [49–51]. The benefits of a DFIG include the low cost of electronic power converters, reduced power losses, variable speed performance, and active and reactive power control, to name a few. Drawbacks include the presence of slip rings, commutation, and its complex model and control scheme. However, controlling the output active and reactive power of a DFIG requires predicting and regulating its electromagnetic characteristics, such as flux and torque. Therefore, various control methods for DFIGs have been introduced [52]. Cascading linear controllers are among the most basic control methods but come with numerous disadvantages. Modern controllers compatible with optimization algorithms are designed to enhance the control performance of these machines, which respond well to traditional methods. The adaptive network-based fuzzy inference system is one of these modern DFIG controllers.

The main difficulty in designing an ANFIS is deciding on its primary parameters, such as membership functions and initial rules. The controller brings the initial selection parameters of membership functions based on the appropriate point of the system's status in the proposed solution. Finally, the controller reduces the torque by selecting the proper torque reference value. The ANFIS controller is recommended for direct power control to reduce torque oscillations at high switching frequencies, which is a significant issue with this method. It also increases the system's resistance to errors and disturbances and the uncertainty of the loads applied.

The wind turbine and DFIG included in the system under study were selected based on a typical case [53,54]; Figure 1. In the block diagram in Figure 1, the stator is connected to the grid, while a back-to-back converter connects the rotor. In typical configurations of the DFIG system, the converters are regulated by a series of proportional–integral (PI) control systems. However, the stability of the PI controller in wind turbines is highly threatened by the increasing system complexity and wind speed deviations. To solve this issue, simultaneous control of the rotor and grid side converters can be used, including a PI controller and an ANFIS method, as proposed in [53]. The wind turbine/DFIG system is fully controllable using the [53] method.
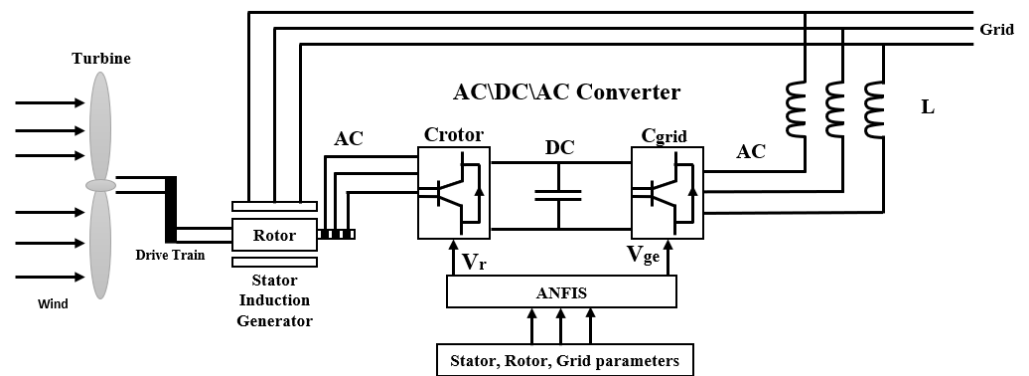

Figure 1. Block diagram of the wind turbine and DFIG system studied in this work.

A model for a DFIG can be defined by a fourth-order differential equation using the $q - d$ coordinate system; Figure 2:

$$V_{qs} = R_s i_{qs} + \omega_e \lambda_{ds} + \frac{d}{dt}\lambda_{qs}, \tag{1}$$

$$V_{ds} = R_s i_{ds} - \omega_e \lambda_{qs} + \frac{d}{dt}\lambda_{ds}, \tag{2}$$

$$V_{qr} = R_r i_{qr} + (\omega_e - \omega_r)\lambda_{ds} + \frac{d}{dt}\lambda_{qr}, \tag{3}$$

$$V_{dr} = R_r i_{dr} - (\omega_e - \omega_r)\lambda_{qr} + \frac{d}{dt}\lambda_{dr}, \tag{4}$$

where $V_{qs}, i_{qs}, V_{ds}, i_{ds}, V_{qr}, i_{qr}, V_{dr}$, and I_{dr} denote the voltages and currents of the stator and rotor in q and d axes, $\lambda_{qs}, \lambda_{ds}, \lambda_{qr}$, and λ_{dr} denote the similar fluxes of the stator and rotor along q and d axes, ω_e denotes the angular (synchronous) speed of the rotary reference frame, ω_r denotes the rotor angular speed, and R_s and R_r denote the stator and rotor resistors, respectively.
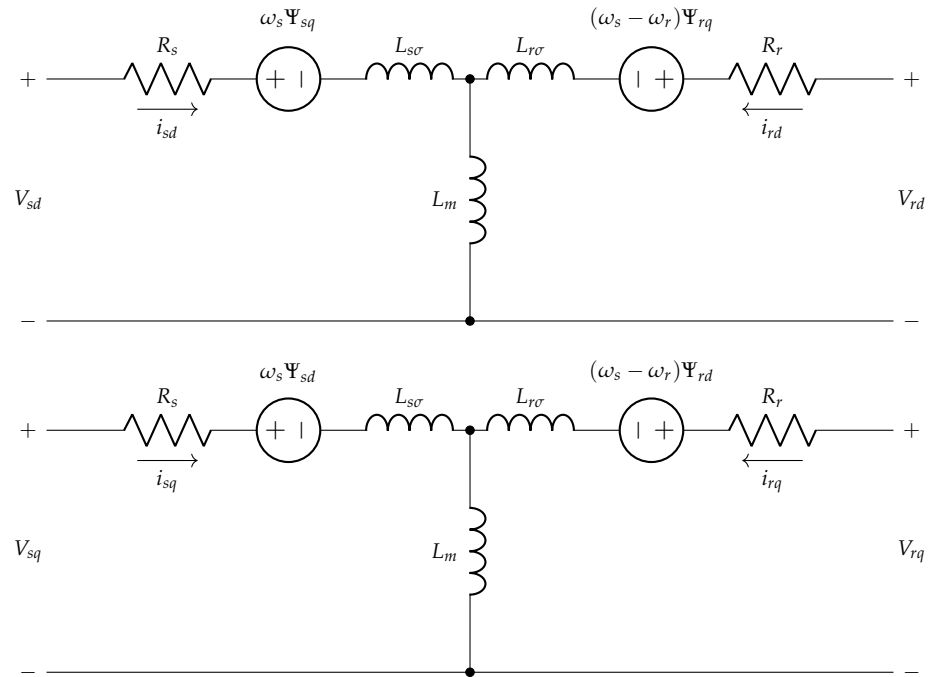

Figure 2. Equivalent circuit of a DFIG.

The linear equations of the currents based on fluxes are as follows:

$$\lambda_{qs} = L_s i_{qs} + L_m i_{qr}, \tag{5}$$

$$\lambda_{ds} = L_s i_{ds} + L_m i_{dr}, \tag{6}$$

$$\lambda_{qr} = L_r i_{qs} + L_m i_{qr}, \tag{7}$$

$$\lambda_{dr} = L_r i_{ds} + L_m i_{dr}, \tag{8}$$

where L_s, L_r, *and* L_m denote the stator, rotor, and mutual inductance. By solving Equations (5) to (8), the currents can be obtained as follows:

$$i_{qs} = \frac{1}{\sigma L_s}\lambda_{qs} - \frac{L_m}{\sigma L_s L_r}\lambda_{qr}, \tag{9}$$

$$i_{ds} = \frac{1}{\sigma L_s}\lambda_{ds} - \frac{L_m}{\sigma L_s L_r}\lambda_{dr}, \tag{10}$$

$$i_{qr} = \frac{1}{\sigma L_s}\lambda_{qr} - \frac{L_m}{\sigma L_s L_r}\lambda_{qs}, \tag{11}$$

$$i_{dr} = \frac{1}{\sigma L_s}\lambda_{dr} - \frac{L_m}{\sigma L_s L_r}\lambda_{ds}, \tag{12}$$

where σ is defined as the leakage factor:

$$\sigma = \left(\left(L_s L_r - L_m{}^2\right)/L_s L_r\right). \tag{13}$$

In some systems, Equations (1) to (4) can be written according to the linkage flux instead of the flux in the per-unit system:

$$V_{qs} = R_s i_{qs} + \frac{\omega_e}{\omega_b} \psi_{ds} + \frac{1}{\omega_b} \frac{d\psi_{ds}}{dt}, \tag{14}$$

$$V_{ds} = R_s i_{ds} - \frac{\omega_e}{\omega_b} \psi_{qs} + \frac{1}{\omega_b} \frac{d\psi_{ds}}{dt}, \tag{15}$$

$$V_{qr} = R_r i_{qr} + \frac{(\omega_e - \omega_r)}{\omega_b} \psi_{dr} + \frac{1}{\omega_b} \frac{d\psi_{qr}}{dt}, \tag{16}$$

$$V_{dr} = R_r i_{dr} - \frac{(\omega_e - \omega_r)}{\omega_b} \psi_{qr} + \frac{1}{\omega_b} \frac{d\psi_{qr}}{dt}, \tag{17}$$

where ψ denotes the linkage flux, and ω_b denotes the base angular speed. In this solution, the rotor side converter feeds a voltage with variable amplitude and frequency to the rotor's winding (Figure 1). In this way, the DFIG system is entirely controllable using the converter. The grid side converter and the ANFIS control the DC link voltage and reactive power. The schematic diagrams, all equations, and a discussion of how these two converters control the parameters of the DFIG and grid are presented in [53]. Regarding the robustness of ANFIS and DFIG systems in wind turbines, refer to Refs. [55,56], which provide valuable insights.

The modeled wind farm is a 9 MW wind farm comprising six 1.5 MW wind turbines connected to a 25 kV distribution system that exports power to a 120 kV grid through a 30 km, 25 kV feeder. The stator winding is connected directly to the grid, while the rotor is fed at variable frequency through the AC/DC/AC converter. The DFIG technology, combined with ANFIS, allows extracting maximum energy from the wind for low wind speeds by optimizing the turbine speed while minimizing turbine mechanical stresses during wind gusts [57]. The maximum and minimum wind speeds in the ANFIS design were assumed as 60 m/s and 4 m/s, respectively. Other implementation features of the two rotor side and grid side converters were defined based on the suggestions presented in [54,58]. Figure 3 depicts the modeled wind farm and the grid, including its transmission line, load, and transformers [54,58].
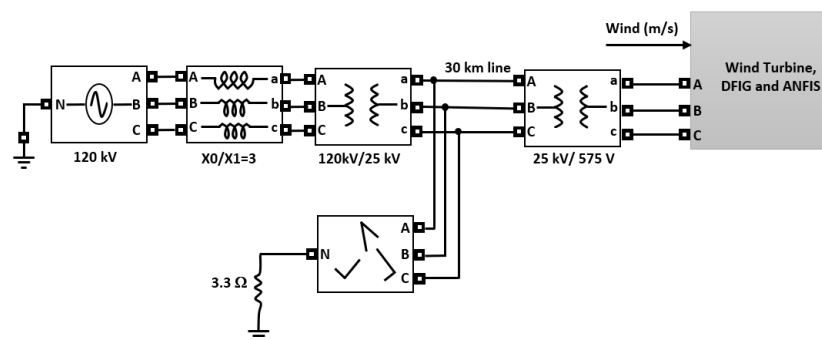
Figure 3. Studied 9 MW wind farm compromising a DFIG and an ANFIS controller.

3.2. PV System

PV systems have three main parts: PV cell, MPPT, and DC/AC converter. Figure 4 shows the PV model used in the present study. The P&O and incremental conductance (INC) algorithms are the control solutions used for MPPT in most hybrid systems [59,60]. Compared to adaptive controllers, these controllers are weaker in flexibility and slow in obtaining the solar cell's MPP but are more simple, applicable, and require less computation. A Z-source converter was used in the current study to connect the solar farms to the grid.
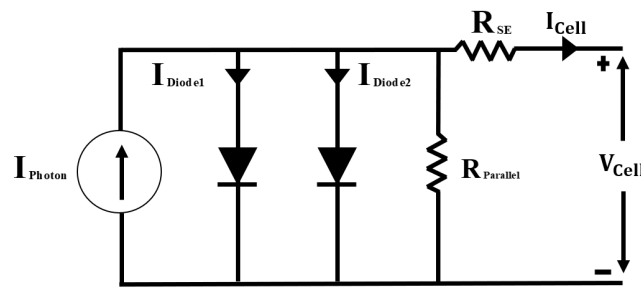
Figure 4. Equivalent circuit of a PV system.

Using the Kirchhoff's current law, the PV cell's output current can be expressed as follows:

$$I_{Cell} = I_{Photon} - I_{Diode1} - I_{Diode2} - \left(\frac{V_{Cell} + I_{Cell} R_{SE}}{R_{Parallel}} \right), \tag{18}$$

where I_{Photon} denotes the source of the circuit, which can be modeled as follows:

$$I_{Photon} = [I_{Photon\_STC} + K_S (T_C - T_{STC})] \times \frac{G}{G_{STC}}, \tag{19}$$

with I_{Photon_STC} denoting the cell currently under standard test conditions (STCs), T_C and T_{STC} denoting ambient and STC temperatures in Celsius, G and G_{STC} denoting the surface and STC irradiance of the cell, and K_S denoting the coefficient of the cell short circuit current, normally provided by its manufacturer [61]. In this study, both the diode reverse saturation currents (Is_i) were assumed equal, therefore:

$$I_{Diodei} = Is_i \left(e^{\frac{V_{Cell} + R_{SE} I_{Cell}}{\eta V_{Thermal}}} - 1 \right), \tag{20}$$

where η denotes ideality factor, a number between 1 and 2 which typically increases as the current decreases and $V_{Thermal}$ is equal to 26 mv. Figure 5 shows the used Z-source converter [62].
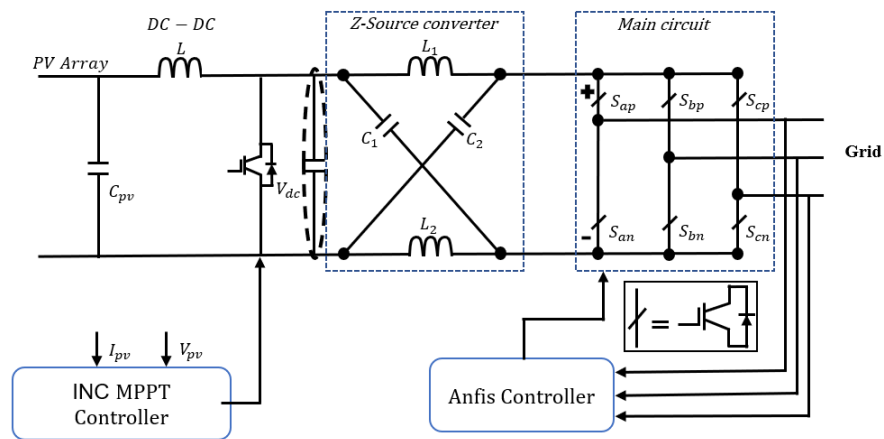

Figure 5. Block diagram of the studied PV and Z-source converter system.

Due to the main circuit state, the Z-source converter operates in two shoot-through and non-shoot-through states. In the shoot-through state, the switches of a phase leg are connected, and in a non-shoot-through state, the upper switch of a phase leg and the lower switch of another phase leg are on. If the capacitors and inductors of the Z-source

impedance network are assumed to be similar, ($C_1=C_2=C$ and $L_1=L_2=L$), the maximum output of the Z-source output can be calculated as follows [63]:

$$\hat{v}_i = V_C - v_L = 2V_C - V_{dc} = \frac{T_{sw}}{T_1 - T_0} V_{dc} = BV_{dc}, \qquad (21)$$

where *B* denotes the boost factor, which can be obtained as follows:

$$B = \frac{T_{sw}}{T_1 - T_0} = \frac{1}{1 - 2(T_0/T_{sw})} = \frac{1}{1 - 2D} \geq 1, \qquad (22)$$

where T_0 and T_1 denote the times of total shoot-through and total non-shoot-through states, respectively, the switching cycle, T_{sw}, is equal to $T_0 + T_1$, and *D* is defined as the shoot-through duty ratio, which is equal to T_0/T_{sw}.

An ANFIS controller and a PWM system were used to control the Z-source converter. The frequency of the modulating signals was assumed to be equal to 60 Hz. Other details of the used Z-source converter can be found in [63]. Two ANFIS controllers in the wind turbine and the PV Z-source converter improve the dynamic response, reduce the power and current fluctuations, increase reliability, and improve the grid voltage profile. Regarding the robustness of solar systems with an ANFIS and Z-source converter approach, Refs. [46,64] confirmed the interesting results. Simultaneously, the current work uses a motion detection algorithm to improve the performance of the incremental conductance (INC) MPPT controller.

3.3. ANFIS Controller

In the current study, the wind turbine, one of the main parts of the studied system, is connected to DFIG and Z-source converter, which are controlled using ANFIS through switching systems (Figure 1). Switching by converters produces voltage and current harmonics, thus increasing power losses in electrical machines. Increasing the switching frequency reduces torque and power ripple. On the other hand, the limited switching frequency for power electronic equipment is necessary to increase the frequency to the desired level. Therefore, other methods must be used to reduce losses and fluctuations in the electric drive system [65]. Several methods have been proposed for controlling DFIGs, particularly the vector and direct control methods [66–68].

The vector control method controls the flux vector, and direct torque and power control methods directly detect the error in DFIG parameters, such as torque, flux, real power, and reactive power, and then set the rotor voltage using pre-defined criteria. An ANFIS controller combines an artificial neural network (ANN) and a fuzzy system. ANNs are mathematical models for fast and accurate processing of information. The ability of ANNs to learn different patterns has led to their widespread use. ANNs transfer data throughout their network structures based on learning processes during data handling. Neural networks can be viewed as electronic models of the human brain, with the foundation of these models being the simulation of neuron activity.

A fuzzy system is based on knowledge and rules. The meaning of knowledge concerns the knowledge of human experts, and the purpose of regulations involves the establishment of rules. Human experience is essential to a fuzzy system, often derived from fuzzy if-then rules. There are two main steps in a fuzzy system, namely, (1) extraction of the rules and (2) combining these rules into a single system known as a fuzzy system. The precise design of a fuzzy controller depends on the high level of experience of the system under study, mainly due to the selection and adjustment of membership functions and their rules. Combining ANN and fuzzy systems can result in a controller with less training data. In this study, aiming to determine the power reference, the DFIG direct power control method was used from an ANFIS controller to reduce the ripple in the speed and torque responses. Additionally, a proportional–integral controller was used to adjust the parameters of the fuzzy elliptic membership functions of the proposed controller. The general plan of the proposed controller was taken from [69], where a type 2 fuzzy neural network was used.

The ANFIS controller proposed for the studied wind turbine is shown in Figure 1. In the proposed scheme, the ANFIS controls both converters. A comprehensive analysis under different scenarios, such as variations in wind speed and super- and sub-synchronous modes, was conducted in the study presented in [53], which validated the performance of the used solution compared to conventional proportional–integral (PI), PI-supervised ANFIS, and model predictive control controllers. On the other hand, the ANFIS controller used for the studied PV system is a modified version of the one suggested in [33].

The block diagram of the proposed PV system, ANFIS controller, and Z-source converter is depicted in Figure 6. The proposed approach, similar to [33], uses the change in power with respect to voltage ($\frac{dp}{dv}$) and the rate of change of power for voltage ($\frac{\Delta dp}{dv}$) as additional input variables. The difference between the proposed approach and that suggested in [33] is the addition of a Z-source converter to convert DC output to AC form. This proposed approach results in a sharper response than usual controllers, leading to robust performance and reduced convergence time for the MPPT controller, which is desirable [33];
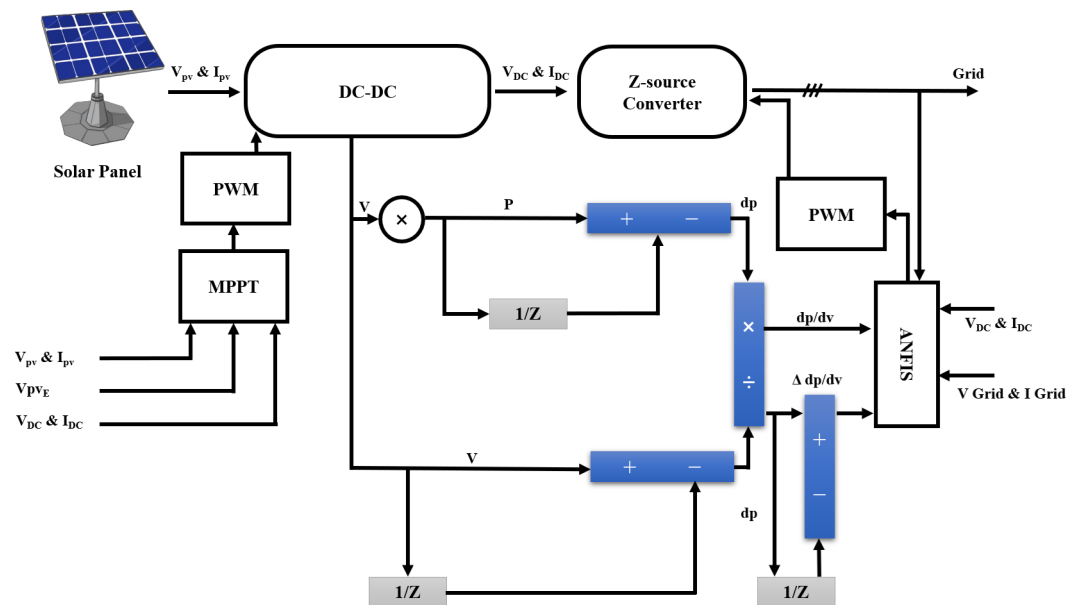

Figure 6. Block diagram of the proposed ANFIS controller for the studied PV system.

The ANFIS controller, Z-source converter, and the main DC-AC converter (Figure 5) regulate the generated voltage before supplying it to the load. In the current study, an extra input to the MPPT block in Figure 6 was added. The usual MPPT controllers only need I_{DC}, V_{DC}, I_{pv}, and v_{pv}. The main novelty of the current study involves adding Vpv_E to the MPPT subsystem, which is based on the cloud's motion prediction.

3.4. MPPT Controller and Motion Detection

The modeled solar element consists of 10 panels, with 72 cells, each one, and arranged in series to generate a total output power of 2.5 kilowatts. The parameters of this structure are given in Table 1.

The required area for installing the proposed structure, which includes 720 PV cells, is approximately 37.5 m^2. This area includes the total space required for installation and access for maintenance. For a 10 MW power plant, 40,000 panels (4000 elements) are required, occupying 15 hectares (150,000 m^2) of total area. The output power curves for this element under different temperatures and irradiation conditions are shown in Figure 7. It is assumed that each panel, comprising 72 solar cells, has its own MPPT. Details of the MPPT system are shown in Figure 8. The proposed MPPT consists of two main MPPT and MPPT subsystem blocks.

Table 1. Parameters of the studied PV system.

Parameter	Value
I_{Short_STC}	8.88 A
Is_1	1 µA
Is_2	1 µA
I_{Photon_STC}	8.88 A
G_{STC}	1000 W/m^2
N_1	1.5
N_2	1.5
R_{SE}	0
$R_{Parallel}$	∞
K_S	0
T_{STC}	25 °C
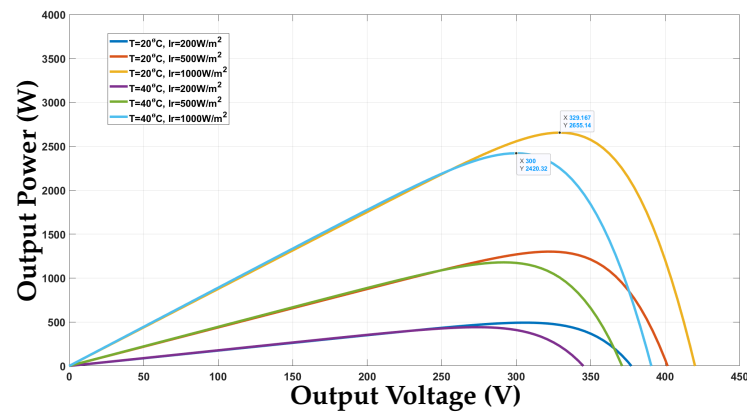
Figure 7. Solar element power curve.
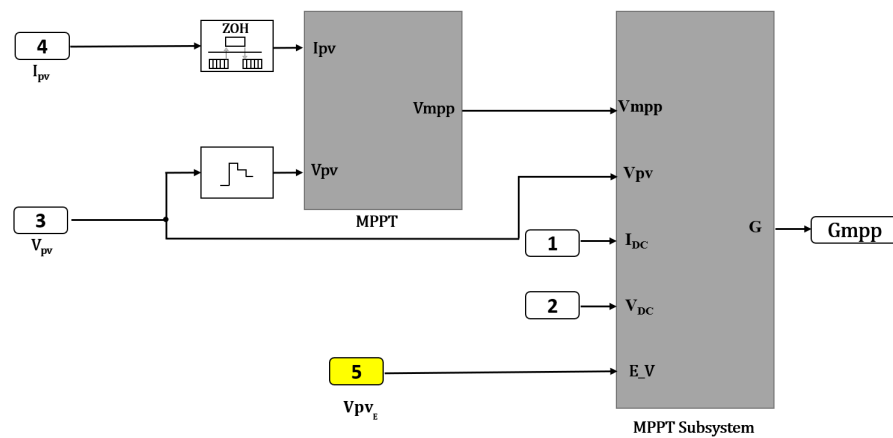
Figure 8. Proposed MPPT controller.

The Vpv_E prediction input was added in the proposed approach to the MPPT subsystem method [70–72] (Figure 8). When the input value of Vpv_E changes, the MPPT algorithm block is bypassed in the first step, and the duty cycle of the controller is updated with the Vpv_E value.

The MPPT algorithm block, which is based on INC, as shown in Figure 9, and the MPPT subsystem, shown in Figure 8, were selected based on a renewable energy example of a solar PV system with MPPT using a boost converter. This setup is available in the Simulink environment of the Matlab R2024a software, with some modifications (see https://www.mathworks.com/help/sps/ug/solar-pv-system-maximum-power-point-tracking-using-boost-converter.html (accessed on 20 September 2024)).
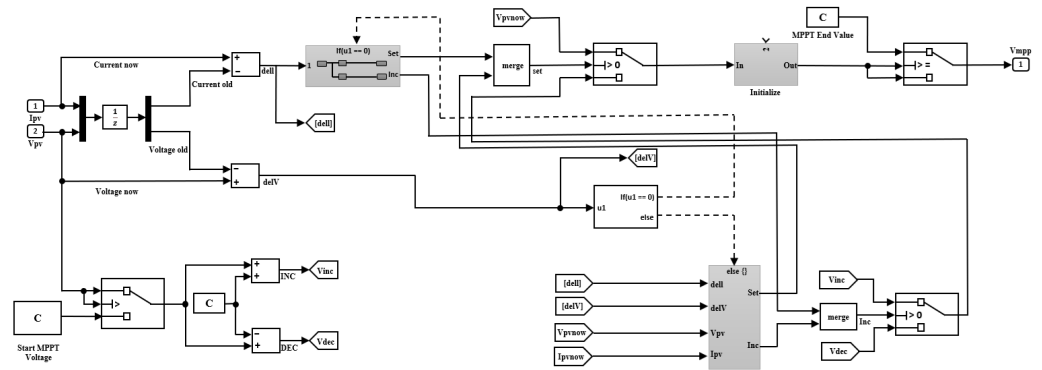
Figure 9. INC MPPT controller.

The proposed approach's main contribution involves adding an extra input (Vpv_E) to the MPPT controller. This input is updated based on the prediction of irradiation changes due to cloud movement across the solar farm. In the current study, the solar farm is modeled as a grid of solar panels (Figure 10), where each panel has a controller. In this figure, the panels are represented by white dots and the remaining area is in black. The grid is assumed to be perfectly regular, with the panel spacing being completely symmetrical. Figure 10b shows the cloud cover entering the solar farm area on a sunny day, which disrupts the irradiation on some of the panels.

Assuming vertical solar radiation, the shadow position on the ground will be as shown in Figure 10c. The proposed approach predicts the movement of the shadow on the panels and, consequently, predicts the changes in the MPPT controller, thus increasing the MPPT speed.
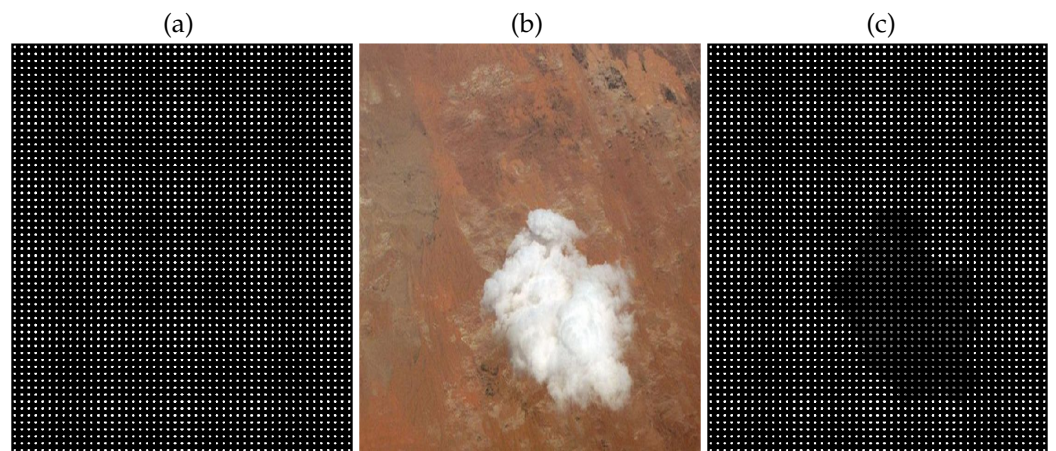
(a)	(b)	(c)

Figure 10. Different aspects of the studied solar farm: (**a**) the model of the solar farm with panels represented by white dots, (**b**) a cloud and its shadow on the solar farm, and (**c**) the solar farm model with shading effects.

The most important advantage of the proposed approach is that it does not require a radiation sensor, as it can detect changes in radiation on the panels based on changes in the PV cell's output. The proposed method can determine changes in radiation by using the output of the solar cells, which directly correlates with the sun's radiation. As shown in Figure 10c, the output of cells in the shaded area changes. In this approach, the proposed method predicts the path of cloud movement and anticipates changes in the MPP of the panels after four time steps. In this manner, the proposed approach can predict the MPP of new panels based on the previous data of other panels before the shadow reaches them. This significantly improves the MPPT INC method speed by updating the Vpv_E. To

detect, locate, and predict the shadow movement in the solar farm area, the 2D normalized cross-correlation (2D NCC) algorithm and linear regression are used.

Since the shaded area causes changes in the panels' output, it is only necessary to track the changes in the MPP to determine the pattern of shadow movement on the solar farm. In the proposed approach, area-based matching algorithms are employed for this purpose. These algorithms assume the area of change to be a rectangular block with variable length and width. To identify the new location of the shadow, the location is first calculated based on changes in the MPPT over several time steps. Then, the future shadow's location is predicted by estimating the new motion vector.

The cross-correlation algorithm is one of the most common and efficient area-based matching algorithms. This method identifies the new shadow region in the secondary image by searching the image window by window, considering its initial pattern. Among the cross-correlation algorithms, NCC was used in this study as follows:

$$2DNCC = \frac{\sum\limits_{v=0}^{R_{length}} \sum\limits_{u=0}^{R_{width}} R(u,v).S(c+u,l+v)}{\sqrt{\sum\limits_{v=0}^{R_{length}} \sum\limits_{u=0}^{R_{width}} R^2(u,v). \sum\limits_{v=0}^{R_{length}} \sum\limits_{u=0}^{R_{width}} S^2(c+u,l+v)}}, \tag{23}$$

where R and S are previously shaded areas and current areas, respectively; the intensity values of these images are selected based on the V_{mpp} value of MPPT controllers; and R_{length} and R_{width} denote the length and width of a previously shaded area. If several shades exist in the solar farm, the NCC (Equation (23)) is calculated for all shades separately to find the best match. Compared to other area-based matching algorithms, correlation-based methods require significantly less computational resources and hardware, making them well-suited for online implementations.

Figure 11 shows shade changes in four-time steps on the solar farm area. The proposed method identifies the location of the shadow in Figure 11 and then obtains the cloud motion vector using the NCC function (Equation (23)).
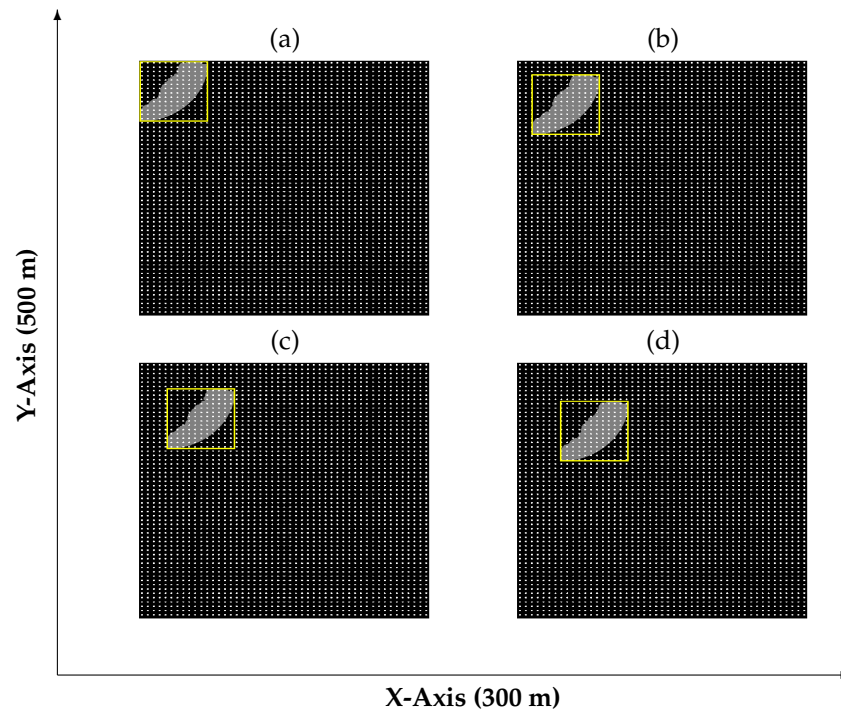
Figure 11. Shade change in four-time steps on the solar farm area (cloud movement from (**a**) to (**d**)—the location of the shadow in the solar farm are indicated by yellow squares).

In the next step, the V_{mpp} values are predicted using the predicted cloud motion vector. Figure 12 shows real motion vectors, represented using squares, and predicted motion vectors, represented using circles on solid lines.
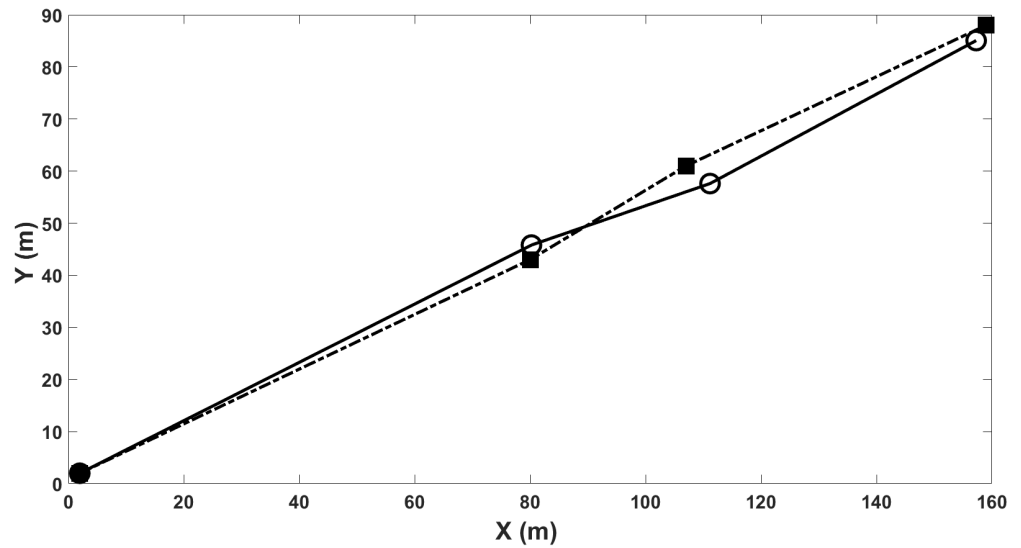

Figure 12. Real (squares on dashed line), and predicted (circles on solid line) motion vectors.

At a glance, the proposed motion estimator predicts the future position of the shadow. Based on this prediction, the central controller predicts the required V_{mpp} voltage for panels and transmits this information to MPPT controllers. This approach enhances the convergence speed of total MPPT controllers without additional sensors. Figure 13 shows the final solution of the proposed system consisting of the DFIG, PV system, battery charger, ANFIS, and Z-source converter.
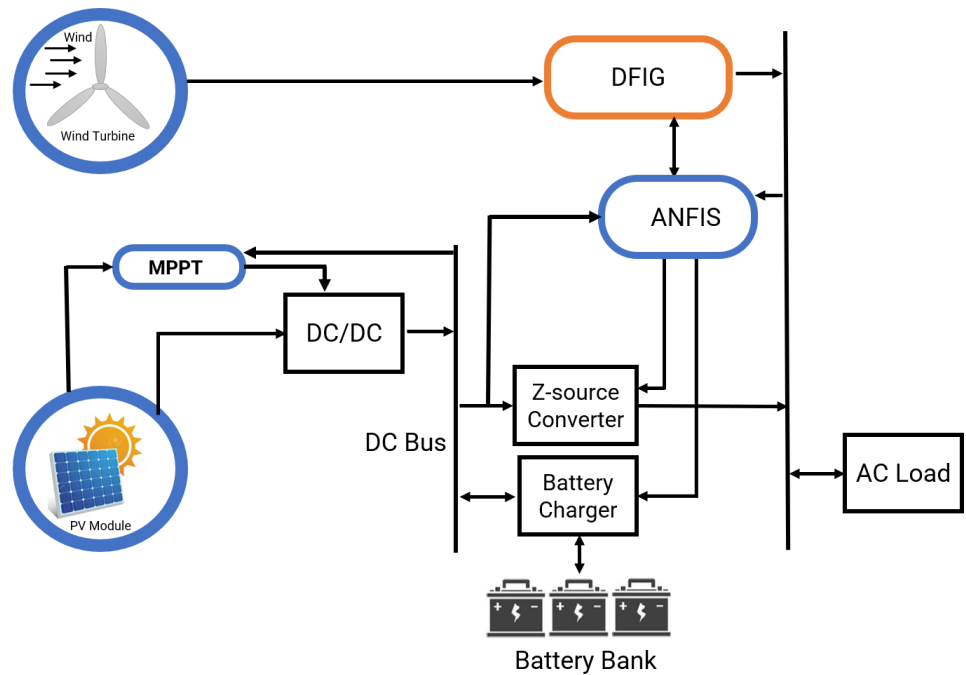

Figure 13. Final solution of the studied system.

3.5. Storage Battery

The proposed system incorporates a storage battery unit in the DC bus, primarily to maintain control circuit operations during power outages. In the absence of wind and sun,

the backup battery ensures the operation of the control circuits. Since both systems are connected to the grid, the battery capacity does not significantly impact power quality and can be determined based on the power consumption of the control circuits. The goal of the storage system is to prevent damage to sensitive and expensive control components when the system is disconnected from the main grid, which could otherwise lead to costly repairs and reduced system output during downtime.

4. Simulation Results

MATLAB/SIMULINK software has been widely used to simulate all types of DFIG and PV systems; it was also used here to evaluate the performance of the proposed system in a hybrid system comprising PV, wind turbine, and battery components. The proposed design consists of three steps. The first step includes the wind turbine, DFIG, and ANFIS; the second is a PV-INC MPPT and Z-source converter; and the last part is the MPPT controller with shadow prediction.

4.1. Evaluation of the Wind Turbine, DFIG and ANFIS

Due to the flexibility of the ANFIS and its applications in various control solutions, it allows for adjustment of the pitch angle of the wind turbine and control of the power injected into the grid under all working conditions. The fuzzy membership functions of the controller were defined based on the stator, rotor, and grid parameters, including the voltage and current of the stator, rotor, and grid, rotor angle, and speed of the stator induction generator (Figure 1).

Figures 14–16 show the wind turbine, DFIG, and ANFIS block output in the input of 25 kV/575 V transformer. The DFIG, transmission line, wind turbine, and load model were selected based on the 9 MW wind farm model of the Matlab R2024a software. The wind speed was taken as 10 m/s and 15 m/s for Figures 14 and 15 and changed from 10 to 15 m/s (Figure 16). The proposed block accurately controlled and stabilized the output voltage in all conditions. The voltage drop between 0.035 to 0.08 s happened because of the initial assumption of load and transmission line events (see Wind Farm DFIG Detailed Model (https://www.mathworks.com/help/sps/ug/wind-farm-dfig-detailed-model.html) (accessed on 20 September 2024)), which is another confirmation of the stability, speed, and robustness of the proposed controller.
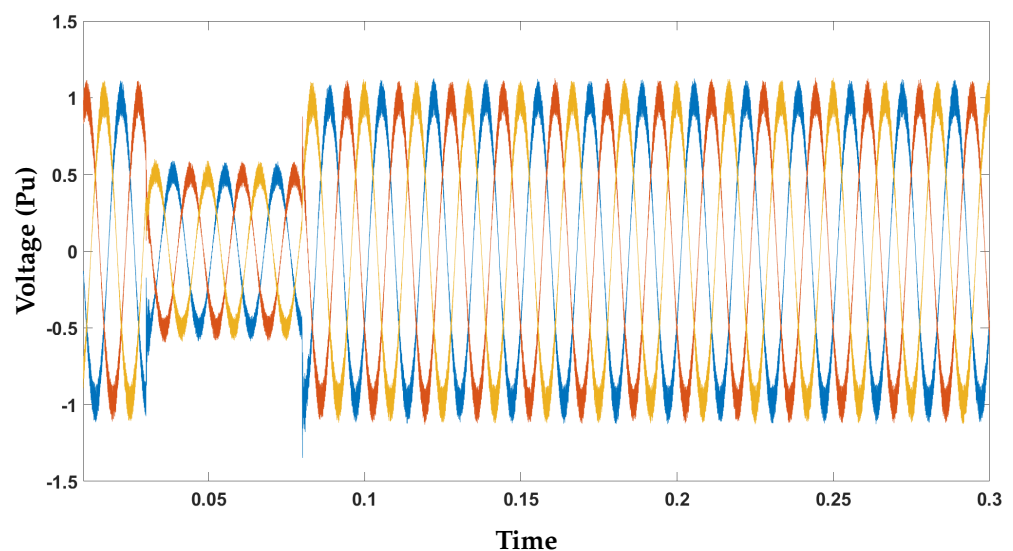

Figure 14. Output voltage (Pu) of the studied wind turbine block with a wind speed of 10 m/s.
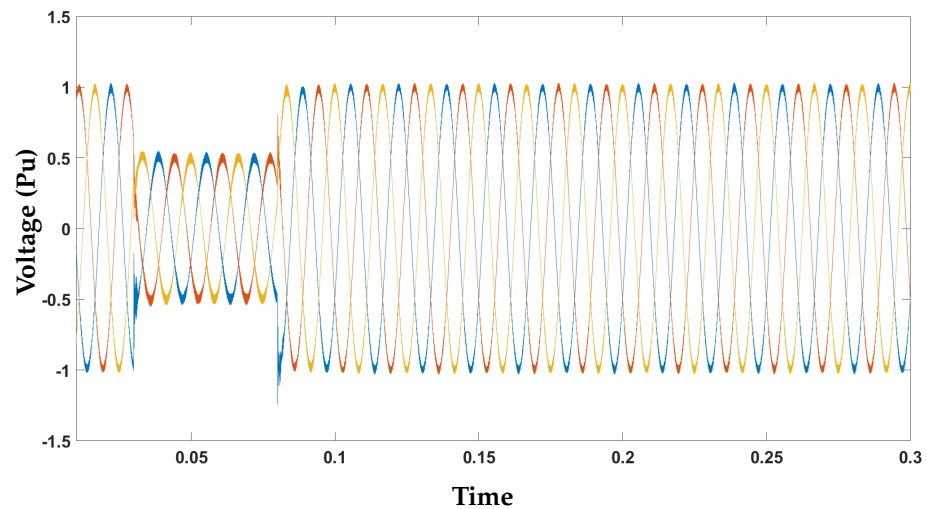
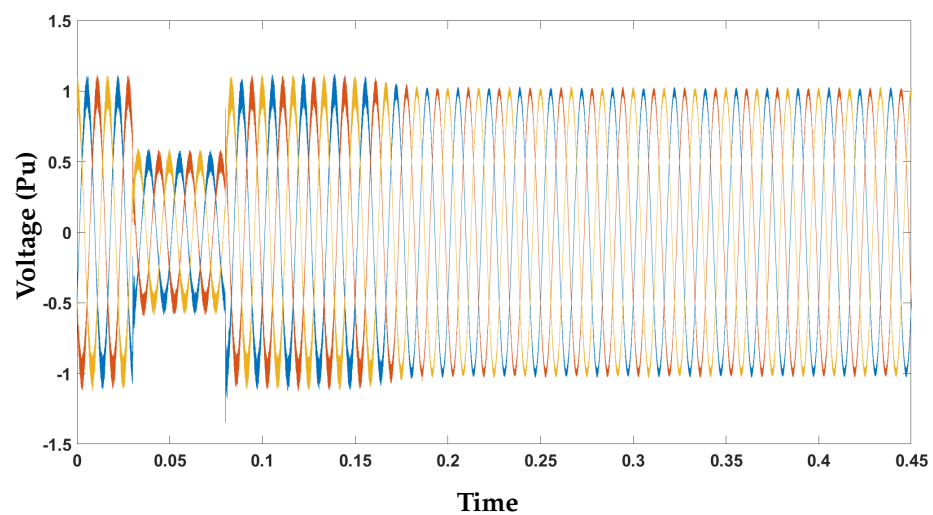**Figure 15.** Output voltage (Pu) of the studied wind turbine block with a wind speed of 15 m/s.

Figure 16. Output voltage (Pu) of the studied wind turbine when the wind speed changes from 10 to 15 m/s.

4.2. Evaluation of the PV System with and Without the Proposed Scheme

The studied PV system was evaluated in two scenarios: with and without the proposed approach. Since the PV system consists of two distinct parts, MPPT and a Z-source converter, and the main contribution is in the MPPT block, the efficiency of MPPT was investigated. Figure 17 shows the changes in the output power of the usual MPPT system under four different irradiance levels. It is assumed that the DC bus absorbs and consumes any values of incoming power. The rated power of the DC bus was 250 watts.

Based on the results from the traditional INC MPPT system, it is observed that at irradiances close to the system's nominal irradiance (1000 W/m^2), the system takes 0.3 s to establish a stable DC bus voltage, and in relatively weak irradiances, such as under heavy shade, it takes about 0.8 s to establish a stable DC bus voltage. Figure 18 shows the boost control signal under different conditions. Zeroing this signal is equivalent to locking the PWM input pulse in its previous state; otherwise, this signal serves as the PWM input. As can be seen from Figure 18, at lower irradiances, the system's response time and the control signal duration are longer. It should be noted that zeroing the control signal is equivalent to maintaining the previous condition in the subsystem, and the system continues to operate based on the last switching time.
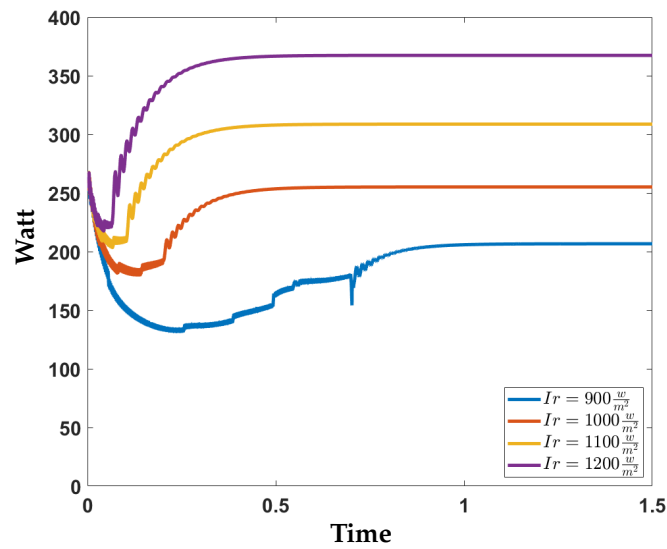
Figure 17. Output power of the studied PV system, including the usual INC MPPT under different irradiance levels.
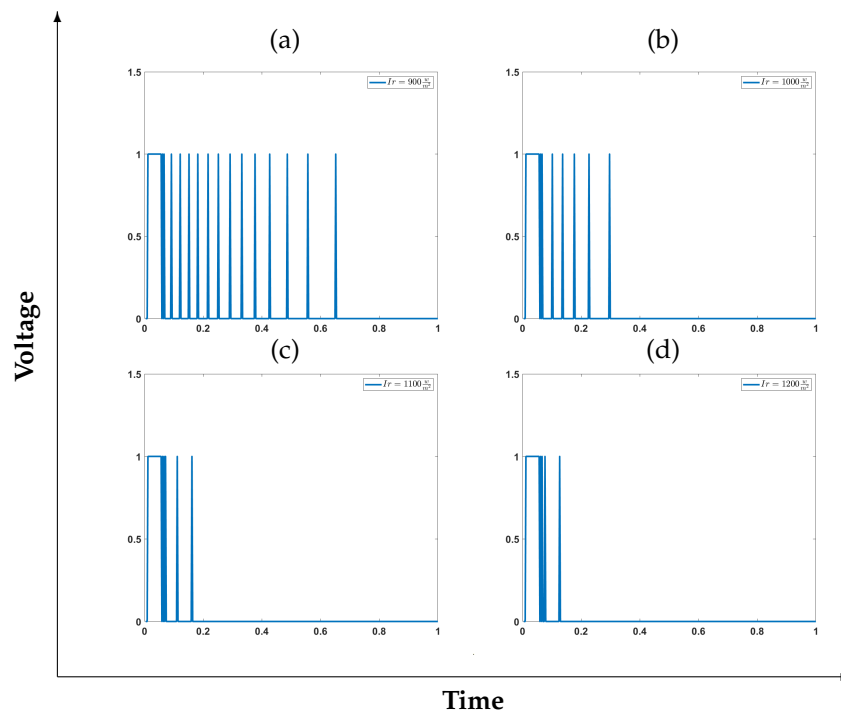

Figure 18. Boost control signal under different conditions: (**a**) 900, (**b**) 1000, (**c**) 1100, and (**d**) 1200 W/m^2.

Figure 19 illustrates the system's performance under reduced irradiance from sunny to shaded conditions. In the case of a moderate shade, the system can reach a steady state within 0.3 s. However, it takes about 1 (one) second under heavy shade conditions to reach a steady state, and the system's output power also significantly decreases.

A prolonged distortion in the range 1250–750 W/m^2 can adversely affect the quality of DC voltage and, consequently, the grid voltage profile, reducing voltage quality. Figure 19b depicts the changes in output during increasing solar radiation, i.e., exiting from the shade. In the case of light shade, the transition to relatively high irradiation occurs quickly, and in the case of exiting from complete shade, it occurs in less than 0.4 s. In this case, the output distortion is lower than in the previous case, indicating a better performance of the MPPT

control under increasing solar radiation. Figure 20 compares two increasing and decreasing irradiation scenarios under similar conditions. It demonstrates that for relatively small changes (Figure 20b), the system's response time is similar for both scenarios.
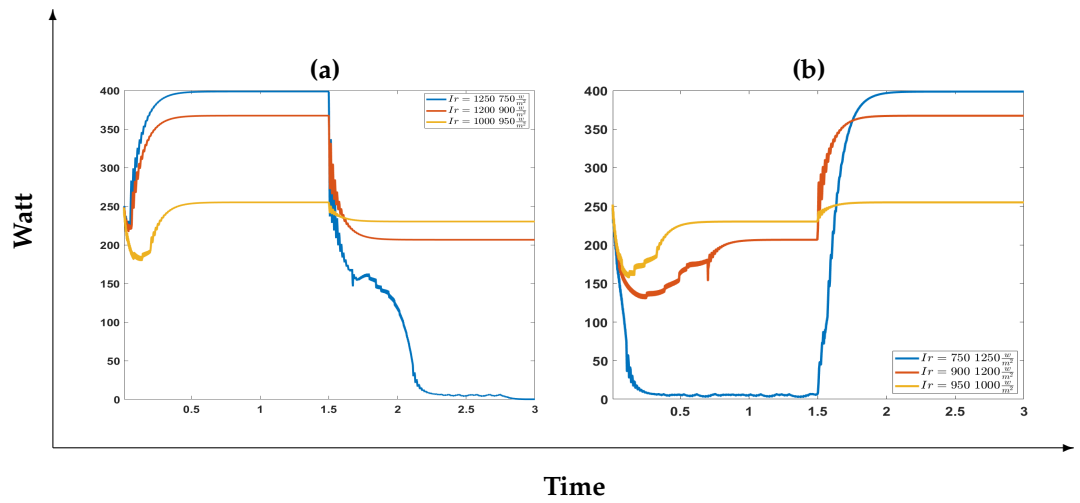

Figure 19. Output power of the studied PV system under two different irradiance conditions: (**a**) reduced irradiance and (**b**) increased irradiance.
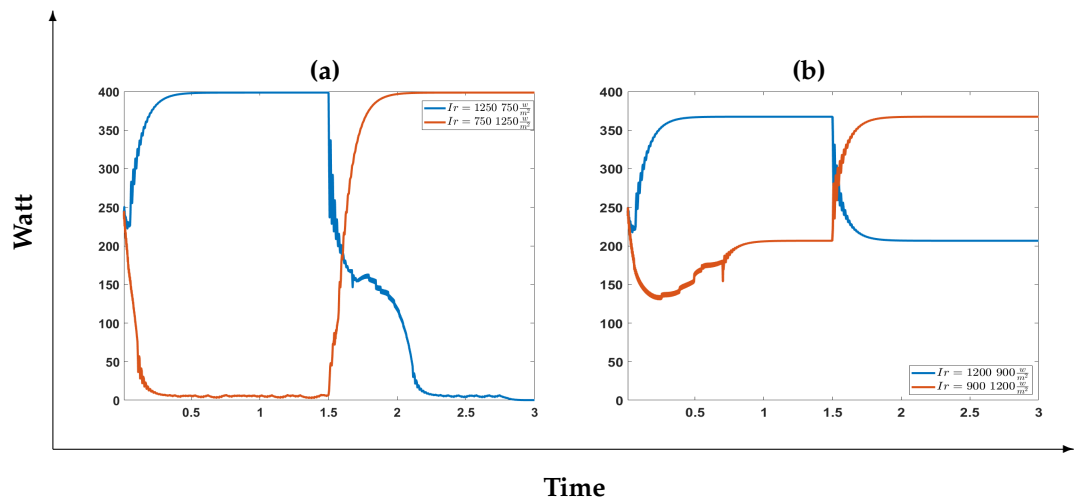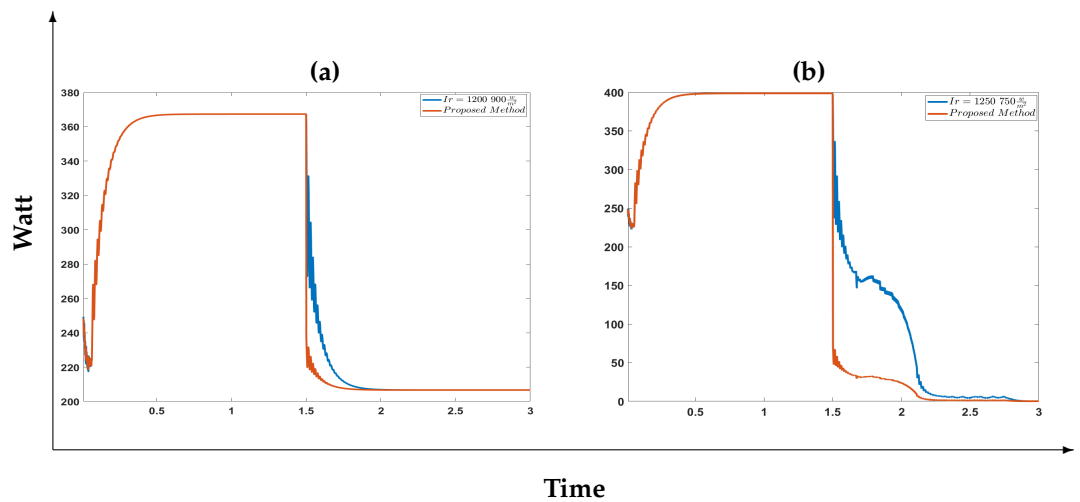

Figure 20. Output power of the studied PV system under two similar increasing and decreasing irradiation conditions: (**a**) $1250 \Leftrightarrow 750$ W/m^2 and (**b**) $1200 \Leftrightarrow 900$ W/m^2.

However, when the irradiance undergoes a significant change and enters the cell's relatively off state (Figure 20a), the system's response to increasing irradiation exhibits less distortion than decreasing irradiation. By applying the proposed approach and predicting MPP, the duty cycle of the boost controller can be estimated and implemented into the system without needing an additional controller. In this scenario, the MPPT block (Figures 8 and 9) is eliminated, and the subsystem block directly determines the duty cycle of the boost controller based on the predicted MPP. To evaluate the PV system's performance against the conventional system, four comparative plots were built (see Figure 21), illustrating their behavior in both shadow-exit and shadow-entry scenarios. As the light irradiation increased—i.e., exiting the shadow—the conventional system exhibited relatively low distortion; however, the proposed method was faster and had significantly lower distortion. Due to the lack of prior prediction during the initial system startup, the proposed MPPT system behaved similarly to the conventional system, showing no difference in performance. In cases of light intensity reduction, the proposed approach proved very effective in reducing the output distortion and response time; Figure 22. The

method significantly reduced even severe distortions, particularly under strong shading conditions. This is because the system's MPP is estimated, and the duty cycle is immediately determined based on that estimation. The response time of the proposed method is only due to the operation of the boost converter during the voltage drop, which effectively reduces the time required to reach the MPP.
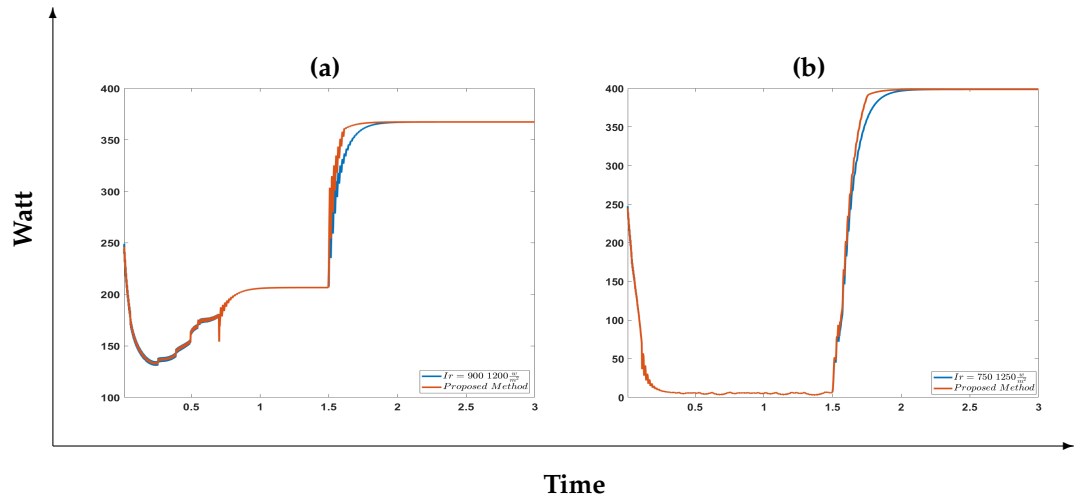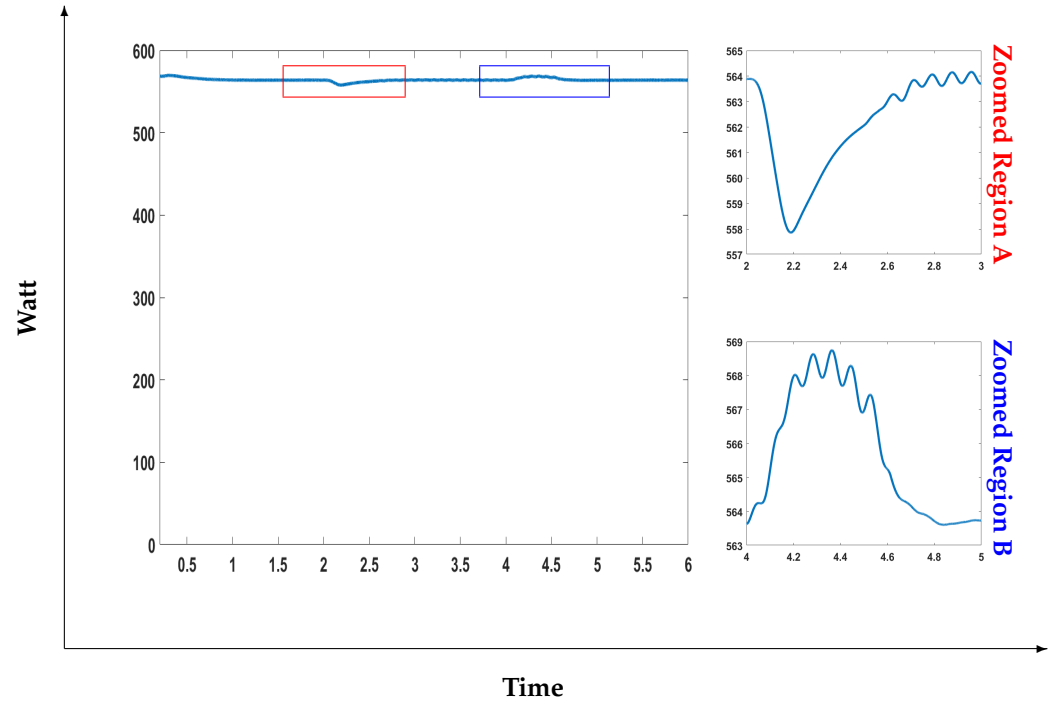

Figure 21. Output power of the proposed and conventional PV system under different irradiation conditions: (**a**) slightly increased irradiation and (**b**) greatly increased irradiation.

Figure 22. Output power of the proposed and conventional PV system under different decreased irradiation conditions: (**a**) slightly decreased irradiation and (**b**) greatly decreased irradiation.

Since conventional methods were used in the other parts of the studied structure, such as in the DC bus-to-grid converters and wind turbine controllers, the related grid stability, voltage profile, distortion, and other grid and load parameters have been evaluated in other research works, such as in [33,53,54,58,63], which confirm their suitability. To demonstrate the effectiveness of the proposed MPPT approach and its impact on the overall structure, further confirmation is necessary.

Figure 23 shows the power output of two solar panels connected in series, under a change in irradiation from 1200 to 900 W/m^2 at $t = 2$ s and then back to 1200 W/m^2 at $t = 4$ s. As shown in Figure 23, the power output had very good stability, and its very small oscillation can be eliminated in the inverter system.

Figure 23. Output power of the studied series of solar panels under a change in irradiation from 1200 → 900 → 1200 W/m^2.

4.3. Advantages of the Proposed Approach

The main advantage of the proposed system lies in its accurate and rapid MPP tracking which leads to enhanced solar farm output, reduced losses, and pressure on the control system. This advantage is clearly illustrated by Figures 24 and 25.
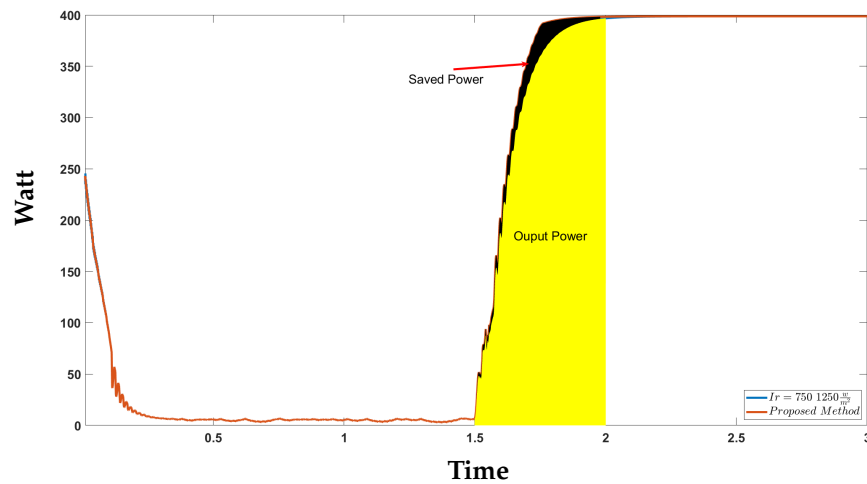
Figure 24. Area under the curve of the output power of the proposed and conventional PV systems under increased irradiation.

Figure 24 illustrates the output power of a studied solar panel on the DC bus in normal mode, represented by the yellow area. If the proposed system functions correctly, the area represented in black is added to the output. In a change similar to that shown in Figure 24, the ratio of the black area to the yellow area, which can be considered an improvement in the output power, is approximately 5%. As Figure 25 shows, when the cell enters a shaded area and the output drops, the system with the proposed controller decreases the voltage more quickly, eliminating the black area represented in Figure 25b. This area can

be interpreted as the pressure applied to the control systems and intermediate circuits to determine the appropriate output of the solar cell. This area is eliminated in the proposed system, and the pressure on the control circuits is reduced by more than 70% while reaching the MPP.
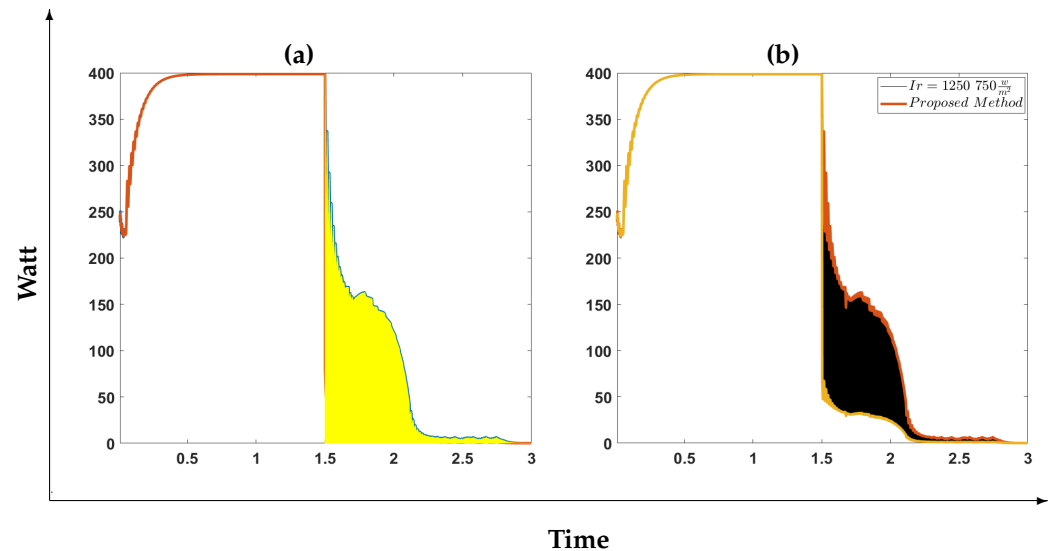
Figure 25. (**a**) Area under the curve of the output power of the proposed (line in red) and conventional (line in blue) PV systems under decreased irradiation, and (**b**) the difference between the two systems (area in black).

In summary, the proposed approach enhances the efficiency of the studied solar power plant in several ways:

- Increased power output during exits from the shadow area: As the irradiation increases, the effective output of the solar farm also rises due to the MPPT improvement.
- Reduced pressure on control circuits during the entrance into the shadow area: When the irradiation decreases or shading occurs, the proposed method reduces the loss and pressure on the control circuits.
- Minimized distortion caused by irregular panel output due to shading: The proposed approach minimizes the DC distortion resulting from irregular panel output caused by shading, ensuring a more regulated power output.

5. Conclusions

This study proposes a shadow movement prediction technique to improve the performance of MPPT controllers in PV systems used in large-scale solar farms. The proposed approach optimizes the MPPT algorithm by predicting the shadow movement pattern in a solar farm, thereby improving the MPPT speed.

The proposed approach does not use any additional sensors and instead uses feedback from the status of existing MPPT controllers in the farm. After the detection of a shade, which is based on a change in the output of the solar panels, the shadow movement is determined after a specified number of time steps. Subsequently, the central controller employs this pattern to predict the shade's movement and gives the information to the MPPT controllers; both panels that will fall under the shade and those that will emerge from it predict MPP based on shadow movement prediction. This approach enhances the MPPT efficiency. The proposed approach uses an image-processing-based motion detection technique using normalized two-dimensional correlation coefficients for shadow movement detection in a solar farm.

A distinctive feature of the proposed approach is its ability to differentiate between the movements of multiple shadows and identify each shadow's location and movement pattern individually. Thus, the approach enhances the performance of MPPT controllers

by accurately predicting shadow movement, optimizing the system's output power in two scenarios: entering or exiting shadow conditions. It increases the system's optimal output power and reduces the pressure on the control set, both in the DC bus and grid connection. The implementation results in a 15-hectare solar farm demonstrated that in shadow conditions with dynamic movement patterns, the output power of the solar panels improved, and the DC distortion in the farm's output was reduced. The simulation results showed that the proposed approach reduces the pressure on the control circuits by more than 70% in the studied 150,000 m^2 solar farm under shaded conditions.

One benefit of the suggested approach is that it uses data from existing MPPT controllers and does not require extra sensors. However, further research is necessary for future studies to accurately assess the efficacy of the proposed approach, particularly considering the potential errors in predicting the MPP due to uncertainties and abrupt changes in cloud movement, as cloud movement patterns and shadow occurrence are completely unpredictable. Future work could also include predicting dust accumulation in windy conditions and adjusting the MPP accordingly. As another practical suggestion, it is important to consider the economic feasibility of implementing this system in a solar farm. In this context, the costs of establishing communication between each solar cell and the central system for output transmission, predicting cloud movement, and how the central system impacts controllers to reach maximum power quickly are crucial. Additionally, security measures to prevent communication disruption between the cells and the central system must also be considered.

Author Contributions: Conceptualization and supervision: J.M.R.S.T.; investigation, data collection, formal analysis, and writing—original draft preparation: A.A.G., V.H., N.S. and M.M.; writing—review and editing: J.J.M.M. and J.M.R.S.T. All authors have read and agreed to the published version of the manuscript.

Institutional Review Board Statement: Not applicable.

Informed Consent Statement: Not applicable.

Data Availability Statement: The data presented in this study are available upon request from the corresponding author due to privacy restrictions.

Conflicts of Interest: The authors declare no conflicts of interest.

References

1. Ai, C.; Zhang, L.; Gao, W.; Yang, G.; Wu, D.; Chen, L.; Chen, W.; Plummer, A. A review of energy storage technologies in hydraulic wind turbines. *Energy Convers. Manag.* **2022**, *264*, 115584. [CrossRef]
2. Barthelmie, R.J.; Pryor, S.C. Climate change mitigation potential of wind energy. *Climate* **2021**, *9*, 136. [CrossRef]
3. Roga, S.; Bardhan, S.; Kumar, Y.; Dubey, S.K. Recent technology and challenges of wind energy generation: A review. *Sustain. Energy Technol. Assess.* **2022**, *52*, 102239. [CrossRef]
4. Attallah, O.; Ibrahim, R.A.; Zakzouk, N.E. Fault diagnosis for induction generator-based wind turbine using ensemble deep learning techniques. *Energy Rep.* **2022**, *8*, 12787–12798. [CrossRef]
5. Bebars, A.D.; Eladl, A.A.; Abdulsalam, G.M.; Badran, E.A. Internal electrical fault detection techniques in DFIG-based wind turbines: A review. *Prot. Control Mod. Power Syst.* **2022**, *7*, 18. [CrossRef]
6. Heng, T.Y.; Ding, T.J.; Chang, C.C.W.; Ping, T.J.; Yian, H.C.; Dahari, M. Permanent Magnet Synchronous Generator design optimization for wind energy conversion system: A review. *Energy Rep.* **2022**, *8*, 277–282. [CrossRef]
7. Touati, Z.; Pereira, M.; Araújo, R.E.; Khedher, A. Integration of switched reluctance generator in a wind energy conversion system: An overview of the state of the art and challenges. *Energies* **2022**, *15*, 4743. [CrossRef]
8. Naveenkumar, R.; Ravichandran, M.; Mohanavel, V.; Karthick, A.; Aswin, L.S.R.L.; Priyanka, S.S.H.; Kumar, S.K.; Kumar, S.P. Review on phase change materials for solar energy storage applications. *Environ. Sci. Pollut. Res.* **2022**, *29*, 9491–9532. [CrossRef]
9. Nasser, M.; Megahed, T.F.; Ookawara, S.; Hassan, H. A review of water electrolysis–based systems for hydrogen production using hybrid/solar/wind energy systems. *Environ. Sci. Pollut. Res.* **2022**, *29*, 86994–87018. [CrossRef] [PubMed]
10. Wang, B.; Yu, X.; Chang, J.; Huang, R.; Li, Z.; Wang, H. Techno-economic analysis and optimization of a novel hybrid solar-wind-bioethanol hydrogen production system via membrane reactor. *Energy Convers. Manag.* **2022**, *252*, 115088. [CrossRef]

11. Rahman, A.; Farrok, O.; Haque, M.M. Environmental impact of renewable energy source based electrical power plants: Solar, wind, hydroelectric, biomass, geothermal, tidal, ocean, and osmotic. *Renew. Sustain. Energy Rev.* **2022**, *161*, 112279. [CrossRef]

12. Zhang, J.; Lu, J.; Pan, J.; Tan, Y.; Cheng, X.; Li, Y. Implications of the development and evolution of global wind power industry for China—An empirical analysis is based on public policy. *Energy Rep.* **2022**, *8*, 205–219. [CrossRef]

13. Owolabi, O.I.; Madushele, N.; Adedeji, P.A.; Olatunji, O.O. FEM and ANN approaches to wind turbine gearbox monitoring and diagnosis: A mini review. *J. Reliab. Intell. Environ.* **2023**, *9*, 399–419. [CrossRef]

14. Goman, O.; Dreus, A.; Rozhkevych, A.; Heti, K.; Karplyuk, V. Improving the efficiency of Darier rotor by controlling the aerodynamic design of blades. *Energy Rep.* **2022**, *8*, 788–794. [CrossRef]

15. Ganthia, B.P.; Mohanty, M.; Maherchandani, J.K. Power analysis using various types of wind turbines. In *Modeling and Control of Static Converters for Hybrid Storage Systems*; IGI Global: Hershey, PA, USA, 2022; pp. 271–286.

16. Wang, J.; Qu, R.; Tang, Y.; Liu, Y.; Zhang, B.; He, J.; Zhu, Z.; Fang, H.; Su, L. Design of a superconducting synchronous generator with LTS field windings for 12 MW offshore direct-drive wind turbines. *IEEE Trans. Ind. Electron.* **2015**, *63*, 1618–1628. [CrossRef]

17. Babaghorbani, B.; Beheshti, M.T.; Talebi, H.A. A Lyapunov-based model predictive control strategy in a permanent magnet synchronous generator wind turbine. *Int. J. Electr. Power Energy Syst.* **2021**, *130*, 106972. [CrossRef]

18. Dwijendra, N.K.A.; Jalil, A.T.; Abed, A.M.; Bashar, B.S.; Al-Nussairi, A.K.J.; Hammid, A.T.; Shamel, A.; Uktamov, K.F. Improving the transition capability of the low-voltage wind turbine in the sub-synchronous state using a fuzzy controller. *Clean Energy* **2022**, *6*, 682–692. [CrossRef]

19. Rodríguez-Amenedo, J.L.; Gómez, S.A.; Martínez, J.C.; Alonso-Martinez, J. Black-start capability of DFIG wind turbines through a grid-forming control based on the rotor flux orientation. *IEEE Access* **2021**, *9*, 142910–142924. [CrossRef]

20. Wankhede, A.K.; Sharma, A.; Fernandes, B. Simulation and Analysis of Medium-Voltage Low-Speed Cyclo-Converter Synchronous Motor Drive and Issues with on-Load Speed Trimming. In *Smart Technologies for Power and Green Energy: Proceedings of STPGE 2022*; Springer: Berlin/Heidelberg, Germany, 2022; pp. 223–233. [CrossRef]

21. Ortatepe, Z.; Karaarslan, A. Robust predictive sensorless control method for doubly fed induction generator controlled by matrix converter. *Int. Trans. Electr. Energy Syst.* **2020**, *30*, e12650. [CrossRef]

22. Rahimi, M.; Asadi, M. Control and dynamic response analysis of full converter wind turbines with squirrel cage induction generators considering pitch control and drive train dynamics. *Int. J. Electr. Power Energy Syst.* **2019**, *108*, 280–292. [CrossRef]

23. Talpone, J.I.; Puleston, P.F.; Cendoya, M.G.; Barrado-Rodrigo, J.A. A dual-stator winding induction generator based wind-turbine controlled via super-twisting sliding mode. *Energies* **2019**, *12*, 4478. [CrossRef]

24. Best, R.J.; Morrow, D.J. Analysis of two-speed wind farm operation from grid-side measurements. *IEEE Trans. Sustain. Energy* **2013**, *4*, 689–697. [CrossRef]

25. Ouhssain, S.; Chojaa, H.; Aljarhizi, Y.; Al Ibrahmi, E.; Hadoune, A.; Maarif, A.; Suwarno, I.; Mossa, M.A. Performance Optimization of a DFIG-based Variable Speed Wind Turbines by IVC-ANFIS Controller. *J. Robot. Control* **2024**, *5*, 1492–1501. . 10.18196/jrc.v5i5.22118. [CrossRef]

26. Zeeshan, A.; Srivastava, S. Fuzzy/ANFIS control of DFIG based wind energy conversion system under the condition of voltage sag on grid in one phase. In Proceedings of the 2024 3rd International conference on Power Electronics and IoT Applications in Renewable Energy and its Control (PARC), Mathura, India, 23–24 February 2024; IEEE: Piscataway, NJ, USA, 2024; pp. 506–513. [CrossRef]

27. Palanivel, M.; Kaithamalai, U.; Parthsarathi, P. Performance assessment of IC and ANFIS based MPPT for PV System using Super Lift Boost Converter. In Proceedings of the 2020 4th International Conference on Electronics, Communication and Aerospace Technology (ICECA), Coimbatore, India, 5–7 November 2020; IEEE: Piscataway, NJ, USA, 2020; pp. 6–11. [CrossRef]

28. Alice Hepzibah, A.; Premkumar, K. ANFIS current–voltage controlled MPPT algorithm for solar powered brushless DC motor based water pump. *Electr. Eng.* **2020**, *102*, 421–435. [CrossRef]

29. Anbarasu, E.; Basha, A.R. An improved power conditioning system for grid integration of solar power using ANFIS based FOPID controller. *Microprocess. Microsyst.* **2020**, *74*, 103030. [CrossRef]

30. Mahdi, A.; Mahamad, A.; Saon, S.; Tuwoso, T.; Elmunsyah, H.; Mudjanarko, S. Maximum power point tracking using perturb and observe, fuzzy logic and ANFIS. *SN Appl. Sci.* **2020**, *2*, 89. [CrossRef]

31. Hamouda, N.; Babes, B.; Kahla, S.; Boutaghane, A.; Beddar, A.; Aissa, O. ANFIS controller design using PSO algorithm for MPPT of solar PV system powered brushless DC motor based wire feeder unit. In Proceedings of the 2020 International Conference on Electrical Engineering (ICEE), Istanbul, Turkey, 25–27 September 2020; IEEE: Piscataway, NJ, USA, 2020; pp. 1–6. [CrossRef]

32. Farah, L.; Haddouche, A.; Haddouche, A. Comparison between proposed fuzzy logic and ANFIS for MPPT control for photovoltaic system. *Int. J. Power Electron. Drive Syst.* **2020**, *11*, 1065. [CrossRef]

33. Javed, M.R.; Waleed, A.; Virk, U.S.; ul Hassan, S.Z. Comparison of the adaptive neural-fuzzy interface system (ANFIS) based solar maximum power point tracking (MPPT) with other solar MPPT methods. In Proceedings of the 2020 IEEE 23rd International Multitopic Conference (INMIC), Bahawalpur, Pakistan, 5–7 November 2020; IEEE: Piscataway, NJ, USA, 2020; pp. 1–5. [CrossRef]

34. Moyo, R.T.; Tabakov, P.Y.; Moyo, S. Design and modeling of the ANFIS-based MPPT controller for a solar photovoltaic system. *J. Sol. Energy Eng.* **2021**, *143*, 041002. [CrossRef]

35. Ibrahim, S.A.; Nasr, A.; Enany, M.A. Maximum power point tracking using ANFIS for a reconfigurable PV-based battery charger under non-uniform operating conditions. *IEEE Access* **2021**, *9*, 114457–114467. [CrossRef]

36. Pareek, S.; Kaur, T. Hybrid ANFIS-PID based MPPT controller for a solar PV system with electric vehicle load. *Proc. IOP Conf. Ser. Mater. Sci. Eng.* **2021**, *1033*, 012012. [CrossRef]

37. Pachaivannan, N.; Subburam, R.; Padmanaban, M.; Subramanian, A. Certain investigations of ANFIS assisted CPHO algorithm tuned MPPT controller for PV arrays under partial shading conditions. *J. Ambient Intell. Humaniz. Comput.* **2021**, *12*, 9923–9938. [CrossRef]

38. Bendary, A.F.; Abdelaziz, A.Y.; Ismail, M.M.; Mahmoud, K.; Lehtonen, M.; Darwish, M.M. Proposed ANFIS based approach for fault tracking, detection, clearing and rearrangement for photovoltaic system. *Sensors* **2021**, *21*, 2269. [CrossRef] [PubMed]

39. Guerra, M.I.; de Araújo, F.M.; de Carvalho Neto, J.T.; Vieira, R.G. Survey on adaptive neural fuzzy inference system (ANFIS) architecture applied to photovoltaic systems. *Energy Syst.* **2024**, *15*, 505–541. [CrossRef]

40. Ahmed, E.M.; Norouzi, H.; Alkhalaf, S.; Ali, Z.M.; Dadfar, S.; Furukawa, N. Enhancement of MPPT controller in PV-BES system using incremental conductance along with hybrid crow-pattern search approach based ANFIS under different environmental conditions. *Sustain. Energy Technol. Assess.* **2022**, *50*, 101812. [CrossRef]

41. Revathy, S.; Kirubakaran, V.; Rajeshwaran, M.; Balasundaram, T.; Sekar, V.; Alghamdi, S.; Rajab, B.S.; Babalghith, A.O.; Anbese, E.M. Design and analysis of ANFIS–based MPPT method for solar photovoltaic applications. *Int. J. Photoenergy* **2022**, *2022*. [CrossRef]

42. Subramaniam, U.; Reddy, K.S.; Kaliyaperumal, D.; Sailaja, V.; Bhargavi, P.; Likhith, S. A MIMO–ANFIS-controlled solar-fuel-cell-based switched capacitor Z-source converter for an off-board EV charger. *Energies* **2023**, *16*, 1693. [CrossRef]

43. Rahman, A.; Myo Aung, K.; Ihsan, S.; Raja Ahsan Shah, R.M.; Al Qubeissi, M.; Aljarrah, M.T. Solar energy dependent supercapacitor system with ANFIS controller for auxiliary load of electric vehicles. *Energies* **2023**, *16*, 2690. [CrossRef]

44. Alaas, Z.; Eltayeb, G.e.A.; Al-Dhaifallah, M.; Latifi, M. A new MPPT design using PV-BES system using modified sparrow search algorithm based ANFIS under partially shaded conditions. *Neural Comput. Appl.* **2023**, *35*, 14109–14128. [CrossRef]

45. Sultana, W.; Jebaseelan, S.S. ANFIS controller for photovoltaic inverter transient and voltage stability enhancement. *Meas. Sens.* **2024**, *33*, 101154. [CrossRef]

46. Sivasubramanian, J.; Veerayan, M.B. ANN and ANFIS Based Control Approaches for Enhanced Performance of Solar PV Driven Water Pumping Systems Employing Quasi Z-Source Converter. *J. Electr. Eng. Technol.* **2024**, *19*, 3499–3513. [CrossRef]

47. Tehrani, K.; Weber, M.; Rasoanarivo, I. Hybrid Power System Optimization for Microgrids. In Proceedings of the 2021 23rd European Conference on Power Electronics and Applications (EPE'21 ECCE Europe), Virtual, 6–10 September 2021; IEEE: Piscataway, NJ, USA, 2021; pp. 1–9.

48. Belgacem, M.B.; Gassara, B.; Fakhfakh, A. Shared energy algorithm and parameters influence on multi-sources and multi-consumers smart microgrid. In Proceedings of the 2019 19th International Conference on Sciences and Techniques of Automatic Control and Computer Engineering (STA), Sousse, Tunisia, 24–26 March 2019; IEEE: Piscataway, NJ, USA, 2019; pp. 578–583.

49. Qin, B.; Li, H.; Zhou, X.; Li, J.; Liu, W. Low-voltage ride-through techniques in DFIG-based wind turbines: A review. *Appl. Sci.* **2020**, *10*, 2154. [CrossRef]

50. Feleke, S.; Satish, R.; Pydi, B.; Anteneh, D.; Abdelaziz, A.Y.; El-Shahat, A. Damping of Frequency and Power System Oscillations with DFIG Wind Turbine and DE Optimization. *Sustainability* **2023**, *15*, 4751. [CrossRef]

51. Benbouhenni, H.; Bizon, N.; Mosaad, M.I.; Colak, I.; Djilali, A.; Gasmi, H. Enhancement of the power quality of DFIG-based dual-rotor wind turbine systems using fractional order fuzzy controller. *Expert Syst. Appl.* **2023**, *238*, 121695. [CrossRef]

52. Karad, S.; Thakur, R. Recent trends of control strategies for doubly fed induction generator based wind turbine systems: A comparative review. *Arch. Comput. Methods Eng.* **2021**, *28*, 15–29. [CrossRef]

53. Moghadam, H.M.; Gheisarnejad, M.; Esfahani, Z.; Khooban, M.H. A novel supervised control strategy for interconnected DFIG-based wind turbine systems: MiL validations. *IEEE Trans. Emerg. Top. Comput. Intell.* **2020**, *5*, 962–971. [CrossRef]

54. Alzubaidi, O.H.A.A.; Dawood, A.Q. Design and Simulation of Wind Farm Model Using Doubly-Fed Induction Generator Techniques. In *Proceedings of the International Conference on Emerging Technologies and Intelligent Systems: ICETIS 2021 (Volume 1)*; Springer: Berlin/Heidelberg, Germany, 2022; pp. 68–78.

55. Kumar, V.; Pandey, A.S.; Sinha, S.K. Stability improvement of DFIG-based wind farm integrated power system using ANFIS controlled STATCOM. *Energies* **2020**, *13*, 4707. [CrossRef]

56. Komijani, H. ANFIS controller design of DFIG under distorted grid voltage situations. *Recent Adv. Electr. Electron. Eng.* **2019**, *12*, 445–452. [CrossRef]

57. Syahputra, R.; Soesanti, I. DFIG control scheme of wind power using ANFIS method in electrical power grid system. *Int. J. Appl. Eng. Res.* **2016**, *11*, 5256–5262.

58. Gagnon, R. *Detailed Model of a Doubly-Fed Induction Generator (DFIG) Driven by a Wind Turbine*; The MathWork: Natick, MA, USA, 2006.

59. Bhattacharyya, S.; Samanta, S.; Mishra, S.; Kumar P, D.S. Steady output and fast tracking MPPT (SOFT-MPPT) for P&O and InC algorithms. *IEEE Trans. Sustain. Energy* **2020**, *12*, 293–302. [CrossRef]

60. Kishor, S.; Rajesh, K.; Rajendrn, S.; Ramkumar, A.; Arunkumar, T. A Comparative Analysis of Maximum Power Point Tracking Algorithms Applied to Hybrid Wind and Solar System. In Proceedings of the 2021 3rd International Conference on Advances in Computing, Communication Control and Networking (ICAC3N), Greater Noida, India, 17–18 December 2021; IEEE: Piscataway, NJ, USA, 2021; pp. 1087–1092. [CrossRef]

61. Horrillo-Quintero, P.; García-Trivi no, P.; Sarrias-Mena, R.; García-Vázquez, C.A.; Fernández-Ramírez, L.M. Model predictive control of a microgrid with energy-stored quasi-Z-source cascaded H-bridge multilevel inverter and PV systems. *Appl. Energy* **2023**, *346*, 121390. [CrossRef]

62. Shid Pilehvar, M.; Mardaneh, M.; Rajaei, A. An analysis on the main formulas of Z-source inverter. *Sci. Iran.* **2015**, *22*, 1077–1084.

63. Peng, F.Z. Z-source inverter. *IEEE Trans. Ind. Appl.* **2003**, *39*, 504–510. [CrossRef]

64. Abu-Rub, H.; Iqbal, A.; Ahmed, S.M.; Peng, F.Z.; Li, Y.; Baoming, G. Quasi-Z-source inverter-based photovoltaic generation system with maximum power tracking control using ANFIS. *IEEE Trans. Sustain. Energy* **2012**, *4*, 11–20. [CrossRef]

65. Mendel, J.M. General type-2 fuzzy logic systems made simple: A tutorial. *IEEE Trans. Fuzzy Syst.* **2013**, *22*, 1162–1182. [CrossRef]

66. Benbouhenni, H.; Bizon, N. Advanced direct vector control method for optimizing the operation of a double-powered induction generator-based dual-rotor wind turbine system. *Mathematics* **2021**, *9*, 2403. [CrossRef]

67. Benbouhenni, H.; Colak, I.; Bizon, N.; Mazare, A.G.; Thounthong, P. Direct vector control using feedback PI controllers of a DPAG supplied by a two-level PWM inverter for a multi-rotor wind turbine system. *Arab. J. Sci. Eng.* **2023**, *48*, 15177–15193. [CrossRef]

68. Parivar, H.; Shivaie, M.; Darahi, A.; Ansari, M. An efficient direct torque control strategy for a doubly fed induction generator (DFIG) in wind energy conversation systems. In Proceedings of the 2021 IEEE Texas Power and Energy Conference (TPEC), Virtually, 2–5 February 2021; IEEE: Piscataway, NJ, USA, 2021; pp. 1–5. [CrossRef]

69. Qiu, J.; Ji, W.; Lam, H.K. A New Design of Fuzzy Affine Model-Based Output Feedback Control for Discrete-Time Nonlinear Systems. *IEEE Trans. Fuzzy Syst.* **2022**, *31*, 1434–1444. [CrossRef]

70. Singh, S.K.; Haque, A. Performance evaluation of MPPT using boost converters for solar photovoltaic system. In Proceedings of the 2015 Annual IEEE India Conference (INDICON), New Delhi, India, 17–20 December 2015; IEEE: Piscataway, NJ, USA, 2015; pp. 1–6.

71. Mohammed, S.S.; Devaraj, D. Simulation of Incremental Conductance MPPT based two phase interleaved boost converter using MATLAB/Simulink. In Proceedings of the 2015 IEEE International Conference on Electrical, Computer and communication Technologies (ICECCT), Coimbatore, India, 5–7 March 2015; IEEE: Piscataway, NJ, USA, 2015, pp. 1–6.

72. Lupangu, C.; Saha, A.; Bansal, R.C.; Justo, J. Critical performance comparison between single-stage and two-stage incremental conductance MPPT algorithms for DC/DC boost-converter applied in PV systems. *Electr. Power Components Syst.* **2022**, *50*, 207–222. [CrossRef]